

Laser Ablation of Poly(ethylene terephthalate)

HIROSUKE WATANABE,¹ MASAHIDE YAMAMOTO²

¹ Fiber and Textile Research Laboratories, Teijin Ltd. Ibaraki-shi, Osaka 567, Japan

² Department of Polymer Chemistry, Graduate School of Engineering, Kyoto University, Kyoto 606-01, Japan

Received 12 August 1996; accepted 25 October 1996

ABSTRACT: Laser ablation of a poly(ethylene terephthalate) (PET) film with an excimer laser beam, 248 nm, was analyzed by various analysis methods, and the mechanism was studied. The ablation was carried out in an argon gas atmosphere at room temperature. Produced gases and some fragments were collected and analyzed by GC-MS. The photochemical fragmentation of PET through the Norrish type I reaction was dominant, but above the threshold fluence, ca. 30 mJ/cm², thermal reactions such as cyclic oligomerization occurred and photochemical fragmentation was accelerated by the thermal energy. © 1997 John Wiley & Sons, Inc. *J Appl Polym Sci* **64**: 1203–1209, 1997

INTRODUCTION

When a polymer film is irradiated with a high-intensity excimer laser, fine ripples are formed on the surface by laser ablation and the chemical composition of the surface is modified. Such laser ablation has been studied extensively. Srinivasan and Braren¹ described the chemical physics of the ablation process on some organic polymers. Bauerle² reported the fundamentals of laser-induced chemical reactions. Lazare and Srinivasan reported the change in surface morphology, surface chemical structure, and surface wettability to water.³ Radical formation on the ablated poly(ethylene terephthalate) (PET) surface has also been reported.^{4,5}

We have studied the laser ablation phenomena from the viewpoints of morphology,⁶ surface chemical structure, and surface properties.^{7–9} PET film is a suitable material for studying the laser ablation since the mechanism of photochemical and thermal reactions have been studied thoroughly. Here, the fragmentation of PET by laser

ablation was studied in detail to clarify the mechanism.

EXPERIMENTAL

Materials

The sample of biaxially drawn PET film (Teijin Co.) was 100 μm thick and was free of additives. The intrinsic viscosity $[\eta]$ was 0.61 in *o*-chlorophenol at 20°C. The value of the carboxyl end group was 35×10^{-6} equiv/g. The surface of all the samples was ultrasonically cleaned in ethyl alcohol and in distilled water for 10 min each and dried for 24 h in a 30°C vacuum dryer before irradiation.

Irradiation with Excimer Laser

Irradiation was carried out with a KrF excimer laser (248 nm) (Lambda-Physik Model LPX120icc) filled with a mixture of Kr, Ne, and F₂ gases. The sample film was cut into a circular form of 4 cm in diameter and put into a glass container with an inner volume of 25 mL. After purging the vial with argon gas, the laser pulse was irradiated on the film through an upper quartz window at a

Correspondence to: H. Watanabe.

© 1997 John Wiley & Sons, Inc. CCC 0021-8995/97/061203-07

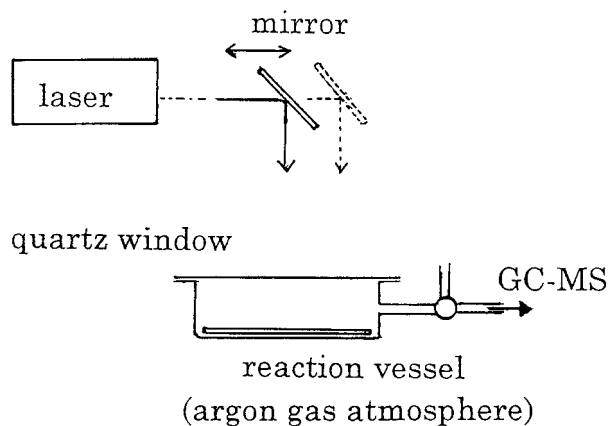


Figure 1 Schematic diagram of the excimer laser irradiation setup.

specified irradiation energy (fluence, 10, 30, and 50 mJ/cm²). The number of irradiated pulses was 5 shots.

Observation of Surface Morphology with SEM

Surface changes before and after laser irradiation were observed by SEM (Nihon Denshi, JEOL Model JSM5300LV), and ablation depth and surface roughness change were measured by an electron probe surface roughness analyzer (Elionix, Model ERA-8000).

Analysis of Chemical Composition (XPS Analysis)

The chemical composition of the surface was analyzed by using ESCA (ESCALAB-200S of V. G. Scientific). The ratio of the oxygen atom to the carbon atom at the surface region was determined from the peak area of the core level spectra of C_{1s} and O_{1s}. By separating overlapping peaks, changes in individual components were measured.

Analysis of Emitted Substances During Ablation

Irradiation was carried out in the atmosphere purged with argon gas; then, the gas was sampled with a syringe and immediately fed into a GC-MS (Hewlett-Packard 5890 Series II and MSD5970) with an analysis column (TC-1701, GL Sciences Inc., diameter 0.25 mm, length 30 m, 80°C). Figure 1 shows a schematic diagram of the laser ablation setup.

Analysis of Ablation Deposits

The deposits on the PET film surface at the time of ablation were collected by washing with acetone, concentrated, and fed to the GC-MS. The analysis was made in the same manner as mentioned above.

RESULTS

Surface Morphology

Figure 2 shows the scanning electron micrographs of the irradiated PET film surface after the laser

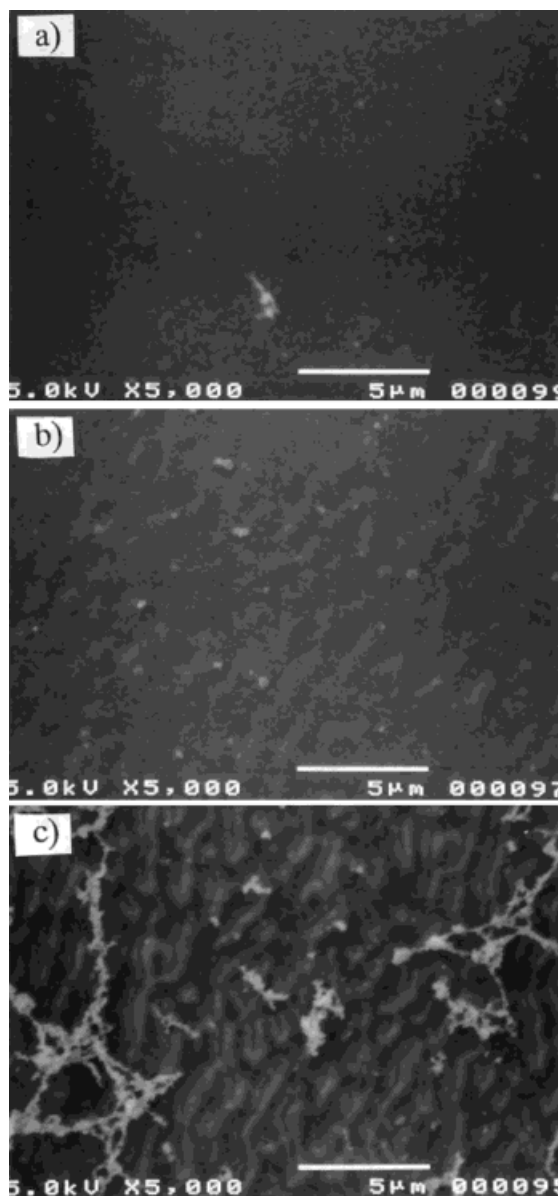


Figure 2 Scanning electron micrographs (SEM) of KrF-irradiated PET film surface after various laser pulse irradiations at (a) 10 mJ/cm² × 5 shots, (b) 30 mJ/cm² × 5 shots, and (c) 50 mJ/cm² × 5 shots.

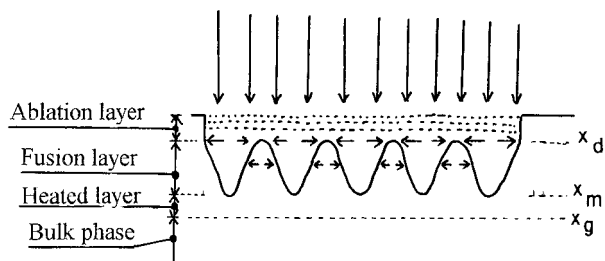


Figure 3 Modified model of PET film surface by excimer laser irradiation, referred to Kesting et al.¹⁰

pulse irradiation at (a) 10, (b) 30, and (c) 50 mJ/cm², with 5 shots. Small ripples were observed when the radiation energy increased above the threshold energy, as reported previously.⁴ However, we found in this experiment that some ablation fragments of PET film deposit on the film surface at high fluences.

Figure 3 shows a schematic model of the ablated polymer surface, which was given originally by Kesting et al.¹⁰ The structure consists of the ablation layer (surface to X_d in diagram), the fusion layer (X_d to X_m), and the layer which was heated above the glass transition temperature (X_m to X_g). Such a surface depth profile was measured by an electron probe surface analyzer, and the depths of the ablation layer and of the fusion layer were calculated. Figure 4 shows the plot of the thickness of each layer against the fluence. The thickness of each layer increased with the increase of irradiation energy. The slope of the ablation layer changed at the fluence of 30 mJ/cm², which indicates the threshold value.

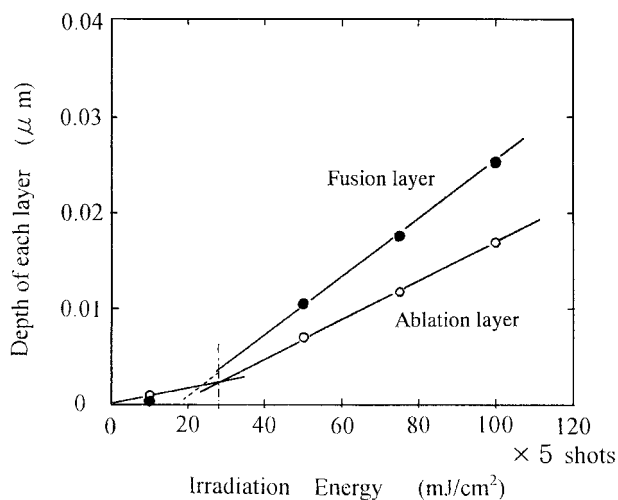


Figure 4 Surface roughness of PET film after excimer laser ablation.

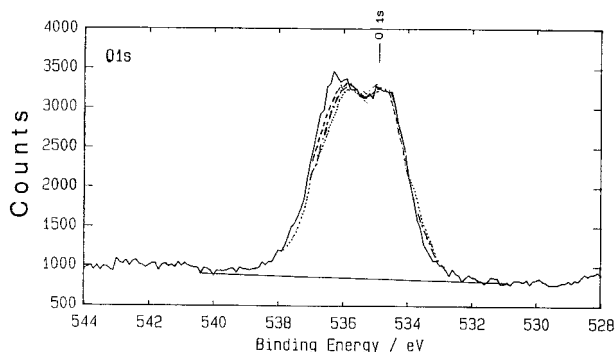
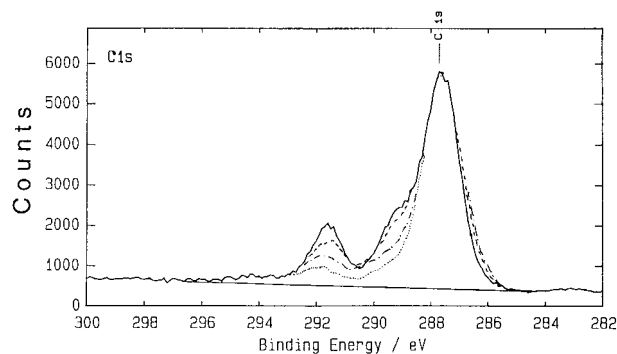


Figure 5 Peak shape change of C_{1S} and O_{1S} by XPS after KrF laser irradiation: (—) nonirradiated; (---) 10 mJ/cm² × 5 shots; (- · - ·) 30 mJ/cm² × 5 shots; (·····) 50 mJ/cm² × 5 shots.

Surface Chemical Composition Studied by XPS Analysis

The content of O and C atoms at the PET film surface after excimer laser irradiation was analyzed by ESCA. Figure 5 shows the narrow scanning spectra of C_{1S} and O_{1S}. As for the C_{1S} spectra, the 287.5 eV peak is normalized, and for the O_{1S} spectra, the 535 eV peak is normalized. The assignment is as follows: C_{1S} 287.5 eV aromatic carbon, 289.5 eV carbon bearing a single oxygen, 291.6 eV carboxylic carbon; O_{1S} 535 eV π -bonded oxygen, 536.4 eV σ -bonded oxygen. The shape of these C_{1S} spectra was carefully examined and was found to change at the 289.5 and 291.6 eV peaks. In particular, both carbon and oxygen peaks were resolved by curve fitting into a sum of single-core levels. Figure 6 shows the relationship between the ratio of O to C atoms and the irradiation energy. With increase of irradiated energy, the O content decreased while the C content increased: This is in agreement with the ones obtained by Lazare and Srinivasan.³ With increase in irradiation energy, the O content became smaller with much dissociation of ester bonds. This finding with the fact that the ratio of the 536.5–535 eV

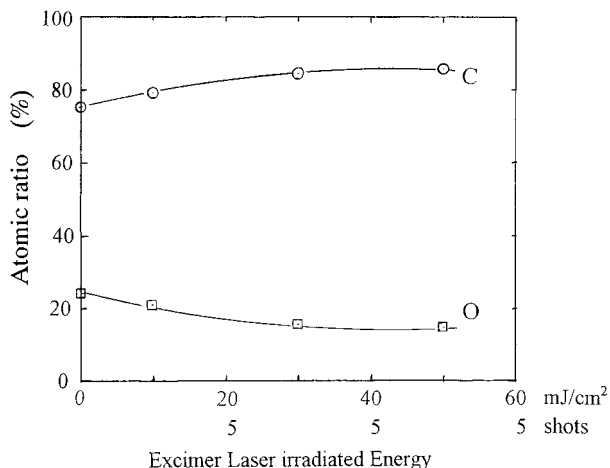


Figure 6 Relationship between the ratio of O to C atoms and irradiation energy.

peak for the O_{1s} spectrum decreased at the same time indicates the deoxidization reaction on the film surface.

Estimation of Ablated Substances

When the PET film in the argon gas atmosphere was irradiated by a KrF laser pulse through a quartz plate, white smoke gas was observed as an ablated substance above a certain fluence. The laser-irradiated area was cloudy, like ground glass, and the surface was undulated under SEM as mentioned above. The ablated substance was sampled and analyzed by GC-MS. Figure 7 shows the obtained mass spectra. The top consists of the reference argon gas with 40 amu. When the sample was irradiated at the fluence below the threshold, 18, 28, 32, 40, and 44 amu peaks appeared, but the intensity was weak. As the fluence was increased, the intensity also increased, and at a high-energy irradiation, new peaks (78, 79, 80 amu) were detected, although the intensity was weak. In these spectra, the intensities of 28 and 44 amu peaks depended on the irradiation energy. The peak of 28 amu is considered to be $CH_2=CH_2$ or/and CO. The peak of 44 amu is assigned to CO_2 . The peak of 78 amu is assigned to C_6H_6 . Figure 8 shows the dependence of the relative intensity on the irradiation energy. The intensity of 28 amu peak did not change much above the fluence of 30 mJ/cm^2 , the threshold fluence, but the satellite peaks changed with the fluence. This threshold value fits well with that reported by Oldershaw.¹¹ The relative intensity ratio of the satellite peak (29 amu) to the main peak (28

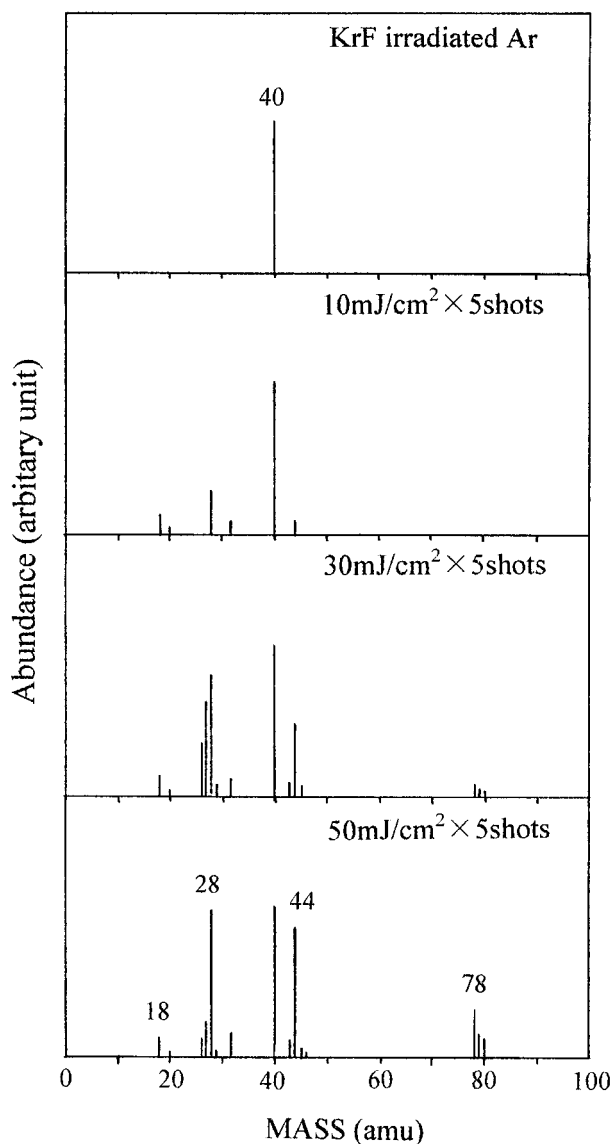


Figure 7 Mass spectra of excimer laser ablated substance.

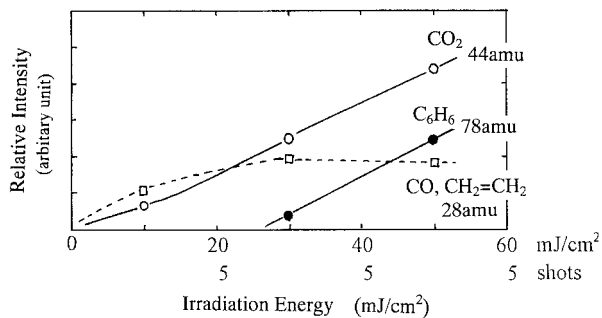


Figure 8 Relative intensity change of mass spectra at 28, 44, and 78 amu.

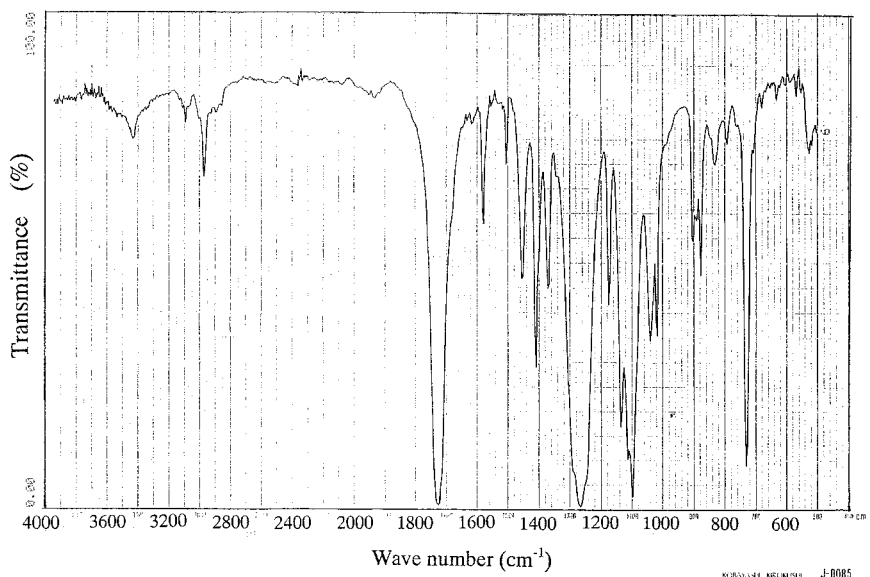


Figure 9 Microscopic FTIR spectra of deposit substance on the PET film.

amu)¹² was large when the fluence was small, but the fluence was large when the ratio was small. This suggests that $\text{CH}_2=\text{CH}_2$ formation is dominant at a low fluence, while the formation of CO is dominant at a large fluence, i.e., depending on the magnitude of the irradiation energy, the reaction of the PET film changes from a conventional photochemical reaction to photochemical fragmentation. On the other hand, the relative intensity of the peak at 44 amu estimated to be CO_2 increased with the increase of irradiation energy. The relative intensity of the peak at 78 amu appeared above the fluence of 30 mJ/cm^2 and increased with the irradiation energy.

With the ablated gases mentioned above, we found a deposited substance on the ablated surface and performed a microscopic FTIR analysis (Fig. 9). The spectra are similar to those of PET, but the bands corresponding to $-\text{OH}$ and $-\text{COOH}$ were absent. The deposited substance was collected by washing with acetone, concentrated, and then analyzed by GC-MS. As Figure 10 shows, a weak peak was observed at 384 amu, a strong peak at 576 amu, and a slightly weak peak at 768 amu. These peaks are attributed to cyclic dimer, cyclic trimer, and cyclic tetramer of PET oligomer, respectively. As for the thermal oligomerization of PET, Burzin et al.¹³ and Cooper and Semlyen¹⁴ extracted the produced cyclic oligomer and analyzed them by gel permeation chromatography. Walker and Semlyen¹⁵ calculated the produced quantity of the cyclic oligomer by the Jacobson and Stockmayer theory using the rotational

isomeric state model. However, their calculated value of the cyclic trimer was smaller than the analyzed one. Aoki simulated the distribution of cyclic oligomers formed in the process of PET polycondensation.¹⁶ KrF excimer laser irradiation induces the cleavage of the ester bond, producing the fragments of $\text{CH}_2=\text{CH}_2$, CO, and CO_2 and depositing PET oligomers on the surface.

DISCUSSION

As for the morphology of PET film surfaces, small ripples appeared as the irradiation energy increased above the threshold energy. In the fusion layer next to the ablation layer, the temperature is above the melting point of PET (ca. 320°C) by

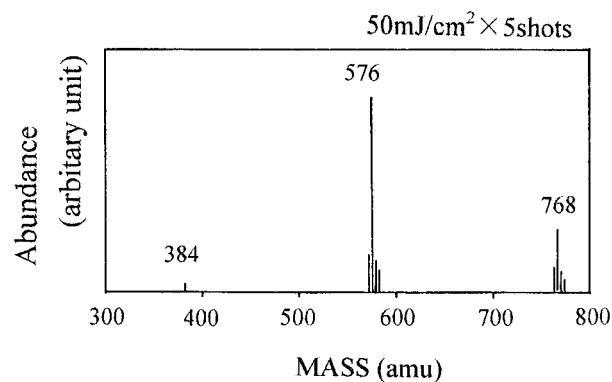
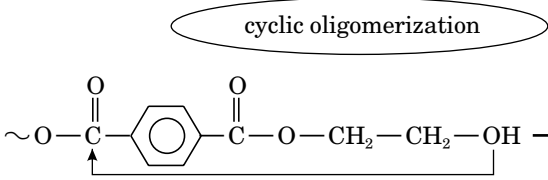


Figure 10 Mass spectra of deposit substance on the PET film.

Table I Characteristics of Laser Irradiation

Irradiation Energy	Ablation Layer	Fusion Layer	
High fluence	Fragmentation (explosive) <div style="border: 1px solid black; border-radius: 50%; padding: 5px; display: inline-block;"> C_6H_6 CO, CO_2 $CH_2=CH_2$ </div>	Deoxidation <div style="border: 1px solid black; border-radius: 50%; padding: 5px; display: inline-block; margin-bottom: 5px;">cyclic oligomerization</div> 	<div style="border: 1px solid black; border-radius: 50%; padding: 5px; display: inline-block;">Radical formation</div> ↓ cyclic oligomers
<Threshold fluence> ca. 30 mJ/cm ²	Fragmentation	Deoxidation Norrish type I	
Low fluence	<div style="border: 1px solid black; border-radius: 50%; padding: 5px; display: inline-block;"> CO, CO_2 $CH_2=CH_2$ </div>		
Conventional light source	No ablation	Norrish type I no oligomerization	

gaining thermal energy and the polymer melts. However, after laser irradiation, they lose energy and are stabilized. At this moment, heat shrinkage of the polymer film occurs, and the mode of stabilization differs at each point depending on the molecular orientation and thermal properties of the polymers. This difference causes the appearance of ripples on the polymer surface.

Day and Willes¹⁷ studied in detail the photodegradation of PET under ordinary photoirradiation. For the polymer having a carbonyl group, cleavage of the chemical bond occurs via a Norrish type I photochemical reaction. Fujimoto and Fujimaki studied the photochemical reactions of PET film with a UV light of 312 nm. They concluded that the photochemical reactions in an air atmosphere occur mainly through photooxidization and that scission takes place via the Norrish type I photoreaction, and hydrogen abstraction, by the radical and subsequent oxidation. They found that the Norrish type II reaction hardly occurs in the solid matrix of PET film.¹⁸ Niino et al. reported that irradiation by the KrF laser generated radicals on the PET film surface although the lifetimes of the radicals were short.⁵ Kokai conducted a similar experiment using irradiation energy above the 200 mJ/cm² fluence, and ionic fragments were observed in addition to neutral fragments.¹⁹ He reported the detection of fragments

of high molecular weights of 230 and 345 amu, respectively. For the production of these ions which have a higher mass than that of the monomer, both ejected fragments from the polymer and reactions of the fragments in the laser-generated plasma may be responsible, as well as the distribution of neutral products.

Table I shows the characteristics of laser irradiation on PET compared with a conventional light irradiation. At the ablation layer, the flux of abundant photons induces the cleavage of bonds, resulting in fragmentation of PET. Under irradiation by the laser pulse, the density of the reaction sites is very high and the reaction is explosive. The photoproducts such as CO, CO₂, and CH₂=CH₂ are produced. At the fusion layer, the high thermal energy accelerates photocleavage reactions, partly with an instantaneous thermal energy; cyclic oligomers are formed and deoxidation occurs. At this layer, various radical species are also generated by photocleavage of the bonds. However, under lower fluences, the photochemical reaction is similar to the conventional photodegradation where the ester bond is cleaved through a Norrish type I reaction; then, it decomposed into smaller fractions. The oxygen loss recorded by the O/C ratio at the fusion layer can be attributed to the loss of small gaseous molecules such as CO and CO₂.

CONCLUSION

Laser ablation of PET films with a 248 nm excimer laser pulse was studied by using various analytical techniques and the ablation mechanism was investigated. Above the threshold fluence, ca. 30 mJ/cm^2 , thermal reactions such as cyclic oligomerization occurred and photochemical fragmentation was accelerated by the thermal energy. This indicates the involvement of thermal reactions at high temperatures in the laser ablation along with photochemical reactions.

REFERENCES

1. R. Srinivasan and B. Braren, *Chem. Rev.*, **89**, 1303 (1989).
2. D. Bauerle, *Laser Processing and Chemistry*, Springer, Berlin/Heidelberg, Germany, 1996.
3. S. Lazare and R. Srinivasan, *J. Phys. Chem.*, **90**, 2124 (1986).
4. P. E. Dyer and J. Sidhu, *J. Appl. Phys.*, **57**, 1420 (1985).
5. H. Niino, T. Imura, C. Nagai, and A. Yabe, *J. Photopolym. Sci. Technol.*, **8**, 461 (1995).
6. H. Watanabe, T. Takata, and M. Tsuge, *Polym. Int.*, **31**, 247 (1993).
7. H. Watanabe, T. Takata, and M. Tsuge, *Sen'i Gakkaishi*, **49**, 157 (1993) (in Japanese).
8. H. Watanabe and T. Takata, *Sen'i Gakkaishi*, **49**, 274 (1993) (in Japanese).
9. H. Watanabe and T. Takata, *J. Adhes. Sci. Technol.*, **8**, 1425 (1994).
10. W. Kesting, T. Bahners, D. Knittel, and E. Schollmeyer, *Angew. Makromol. Chem.*, **212**, 129 (1993).
11. G. A. Oldershaw, *Chem. Phys. Lett.*, **186**, 23 (1991).
12. J. H. Beynon, *Mass Spectroscopy and Its Application to Organic Chemistry*, Elsevier, Amsterdam, 1960.
13. K. Burzin, W. Holtrup, and R. Feinauer, *Angew. Makromol. Chem.*, **74**, 93 (1978).
14. D. R. Cooper and J. A. Semlyen, *Polymer*, **14**, 185 (1973).
15. G. R. Walker and J. A. Semlyen, *Polymer*, **11**, 472 (1970).
16. (a) H. Aoki, *Kobunshi Ronbunshu*, **51**, 275 (1994) (in Japanese); (b) **51**, 283 (1994).
17. M. Day and D. M. Willes, *J. Appl. Polym. Sci.*, **16**, 191 (1972).
18. E. Fujimoto and T. Fujimaki, *Kobunshi Ronbunshu*, **52**, 378 (1995) (in Japanese).
19. F. Kokai, *J. Photopolym. Sci. Technol.*, **5**, 297 (1992).